



RESEARCH MEMORANDUM

INVESTIGATION OF FLUTTER CHARACTERISTICS OF THREE
LOW-ASPECT-RATIO ALL-MOVABLE HALF-SPAN CONTROL
SURFACES AT MACH NUMBERS FROM 1.49 TO 2.87

By Homer G. Morgan, Irving E. Figge,
and John G. Presnell, Jr.

Langley Aeronautical Laboratory
Langley Field, Va.

LIBRARY COPY

MAY 5 1958

LANGLEY AERONAUTICAL LABORATORY
LIBRARY, NACA
LANGLEY FIELD, VIRGINIA

CLASSIFIED DOCUMENT

This material contains information affecting the National Defense of the United States within the meaning of the espionage laws, Title 18, U.S.C., Secs. 793 and 794, the transmission or revelation of which in any manner to an unauthorized person is prohibited by law.

NATIONAL ADVISORY COMMITTEE FOR AERONAUTICS

WASHINGTON

May 2, 1958

PHS 7 261480
76-1244



~~CONFIDENTIAL~~

NATIONAL ADVISORY COMMITTEE FOR AERONAUTICS

RESEARCH MEMORANDUM

INVESTIGATION OF FLUTTER CHARACTERISTICS OF THREE
LOW-ASPECT-RATIO ALL-MOVABLE HALF-SPAN CONTROL
SURFACES AT MACH NUMBERS FROM 1.49 TO 2.87

DNASH COND-#880

By Homer G. Morgan, Irving E. Figge,
and John G. Presnell, Jr.

10-12-66
11-8-66
bmd

SUMMARY

Results of a supersonic flutter investigation of three low-aspect-ratio control surfaces are presented in this paper. Two controls were all-movable but the third had a fixed cutout. The test was conducted in the low Mach number test section of the Langley Unitary Plan wind tunnel. The Mach number range was 1.49 to 2.87. Various ratios of uncoupled bending frequency to uncoupled pitching frequency were used. Some of the models tested had a mass balance. Results show that flutter may be eliminated or the dynamic pressure at flutter may be increased by the use of mass balance. It was also found that the lowest flutter dynamic pressures were obtained when the ratio of the uncoupled bending frequency to the uncoupled pitching frequency was near 1. Some calculations using piston theory are presented and compared with experiment.

INTRODUCTION

Flutter of control surfaces has long been a problem of concern to the aircraft designer. In the past, for subsonic flight, certain flutter variables have been found to be important. Procedures for overcoming or preventing control-surface flutter, such as mass-balancing, control of stiffnesses, or control of frequency ratios, have been developed. As flight speeds become higher, the problem arises as to whether or not these same flutter-prevention procedures are applicable for supersonic flight. In the absence of proven calculation procedures and experience on a large variety of configurations for supersonic flight, proposed control surfaces for high-speed vehicles must usually be tested for flutter.

~~CONFIDENTIAL~~

Three elevator plan forms which were being considered for a high-speed ground-to-air missile have been tested in the Langley Unitary Plan wind tunnel over the Mach number range from 1.49 to 2.87 to determine their flutter characteristics and to evaluate the relative merits of the plan forms. Mass-balancing as a possible flutter alleviator on an all-movable control was investigated by using two types of balance weights - a weighted boom and a weighted leading edge. Several ratios of uncoupled bending frequency to uncoupled pitching frequency were also investigated by varying the pitching restraint of a simulated actuator.

Flutter calculations have been made on one of the plan forms for comparison with experiment. The structural portion of the flutter analysis was handled by using both coupled and uncoupled vibration modes. Piston theory was chosen from several theories to give the aerodynamic input because of its simplicity and inclusion of airfoil-thickness terms. Structural damping is included in some of the calculations. It may be noted that a summary of some of the results for the control configurations given herein was included in the survey study given in reference 1.

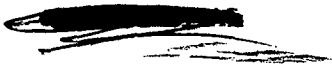
SYMBOLS

a	speed of sound, fps
b	one-half chord, ft
F_h	bending-mode deflection along rotation axis
F_θ	pitching-mode deflection
f	frequency, cps
g	structural-damping coefficient
I_θ	mass moment of inertia per unit length about axis of rotation, $\frac{\text{slug-ft}^2}{\text{ft}}$
l	total semispan along hinge axis, ft
M	Mach number
m	mass of control per unit length, <u>slugs/ft</u>

- q dynamic pressure, $\frac{1}{2}\rho V^2$, lb/sq ft
 S_θ static unbalance of wing per unit length about axis of rotation, positive rearward of center of gravity, $\frac{\text{slug-ft}}{\text{ft}}$
 V velocity, fps
 η distance from root of control along hinge axis, fraction of span
 μ ratio of mass of control to mass of air contained in cone determined by control, $\frac{\text{Mass of control}}{\rho l \pi \int_0^1 b^2 d\eta}$
 ρ air density, slugs/cu ft
 ω circular frequency, radians/sec

Subscripts:

- c calculated
 e experimental
 f value at flutter
 h uncoupled bending
 θ uncoupled pitching
 r reference mean aerodynamic chord
 1 first coupled mode
 2 second coupled mode


APPARATUS AND MODELS

Apparatus

The investigation was conducted in the low Mach number test section of the Langley Unitary Plan wind tunnel. This tunnel is a variable-pressure, continuous, return-flow type. The test section is 4 feet square and approximately 7 feet in length. The nozzle leading to the test section is of the asymmetric sliding-block type. The Mach number can be varied continuously through a range from approximately 1.49 to 2.87.

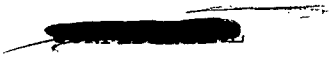
A drawing illustrating the test setup is shown in figure 1. Boundary-layer effects were minimized by projecting the model outside the boundary layer with a fixed strut. The supporting mechanism of the models was mounted on a removable turntable located in the tunnel wall. A torque tube operating in low-friction bearings was mounted to the elevator surface and passed through the tunnel wall. The models were restrained in pitch by a spring that was instrumented with a strain gage. This system allowed the pitching frequency of the model to be varied. The entire mounting mechanism was housed in a pressure-sealed container. A photograph of a model installed in the test section is shown in figure 2.

Both low- and high-speed cameras recorded elevator flutter. The motion pictures aided in determining the flutter modes. A high-speed camera operated at 2,000 frames per second, and another camera operated at 180 frames per second.

Models

Configuration.- Three low-aspect-ratio half-scale elevator plan forms were tested. Two control plan forms were all-movable but the third control had a fixed cutout. Details of these models are shown in figure 3, and the geometric characteristics are given in table I. Photographs of the models are presented in figure 4. All plan forms had circular-arc airfoil sections, modified over the truncated portion of the plan forms to have a blunt trailing edge. Strain gages were located on all models at the positions shown in figure 3 for flutter-frequency determination. These strain gages were mounted internally on ribs and spars.

Plan-form 1 was a 5-percent-thick, spindle-mounted, all-movable control surface whose axis of rotation was at the 38-percent mean-aerodynamic-chord station. In addition to the basic control, two types of mass-balancing were provided for this model. One balance was



a weighted leading edge which increased the weight of the control by 20 percent. The second type of balance weight was boom-mounted (see figs. 3(a) and 4(a)) at the 60-percent-span station. The added weight when the boom was used, including the boom, was about $18\frac{1}{2}$ percent of the basic model weight.

Plan-form 2 was also spindle-mounted but its axis of rotation was at the 45-percent mean-aerodynamic-chord station. Thickness varied linearly from 6 percent at the root to about $3\frac{1}{2}$ percent at the tip. The basic elevator was designed to have as little mass unbalance about the hinge line as possible. One variation that was studied on the model was a heavy leading edge on the outboard 48 percent span of the control, as shown in figure 3(b). This increased the model weight by about 7 percent.

Plan-form 3 was mounted on a hinge tube carried by a fixed stub which was 25 percent of the total surface area. The control hinge line was at the 42-percent mean-aerodynamic-chord station, and the model was 3 percent thick.

Construction.- The structure of all models was similar to that of full-scale control surfaces. Plan-forms 1 and 2 had conventional rib and spar construction with duralumin skin. Their steel spindles were supported by two needle bearings. Plan-form 3 was of duralumin-honeycomb construction with duralumin skin. This control rotated in two ball bearings which were attached to the spar of the fixed stub. On all models the pitching restraint of an actuator was simulated by springs attached at the location shown in figure 3. These springs could be changed to vary the pitching frequency. The bending frequency was determined by the spindle or stub spar and remained essentially constant.

Physical parameters.- The mass parameters of the models studied are given in table II. The listed weights do not include the part of the spindle which is outside the surface, nor do they include the pitch spring. The calculated mass, static-unbalance, and moment-of-inertia distributions for plan-form 2 are given in table III.

The vibration modes and frequencies were investigated on the models, prior to installation in the tunnel, by using an electromagnetic shaker and small accelerometers. Mode shapes were found on most of the models by exciting the model at a resonant frequency and measuring displacements with the accelerometers. Coupled modes and frequencies were found with the model unrestrained except for the pitch spring. Uncoupled modes and frequencies were found by restraining the model to lock out unwanted response. Uncoupled pitching was found by holding the model on its pitch axis near the tip, and uncoupled bending was found by clamping the model at the root, off the hinge line.

Measured coupled and uncoupled modes for two uncoupled-frequency ratios on plan-form 2 are given in table IV and figure 5. As this table and figure show, most of the pitching deflection was pure rotation with small amounts of twist in the surface. The bending deflection had large components of both elastic deformation of the surface and flapping about the root. Structural-damping coefficients were determined from the decrement of free vibrations in still air at the frequency of the mode of interest.

TEST TECHNIQUES

Models were mounted in the test section at zero angle of attack. After mounting, the pretest procedure consisted of a brief resonant vibration test to check the pitching and bending frequencies of the models.

Test results were obtained by operating the tunnel at a constant Mach number and increasing the stagnation pressure until flutter was obtained or the maximum tunnel operating conditions were reached. If the model fluttered, stagnation pressure was reduced until flutter ceased.

During the test program, it was found that the dynamic pressure at the end of flutter was often much less, by as much as 50 percent, than the dynamic pressure at the start of flutter. Thus, two test points were obtained - one when flutter was initiated and another when flutter stopped. It was found that flutter could be started at lower dynamic pressures if turbulence were introduced into the airstream by opening an air inbleed valve upstream from the test section. The implications of this procedure are discussed in a later section.

The start or stop of flutter was determined by observing an oscilloscope on which bending and pitching strain-gage signals were displayed on the horizontal and vertical axes, respectively. At flutter, the amplitude increased rapidly and the frequency from both gages became the same; thus, an elliptical pattern was given on the oscilloscope. Time histories of the pitching and bending strain-gage signals were then recorded on high-speed oscillographs.

The tunnel-data recording system was used to obtain Mach number, dynamic pressure, and stagnation temperature when flutter started, when it stopped, or when maximum dynamic pressure was reached if no flutter occurred during the test.

ANALYSIS

Flutter-speed calculations were made on plan-form 2 for comparison with experiment. The equations of motion of the system were derived in reference 2; however, supersonic aerodynamic coefficients must be used herein. The first two measured vibration modes and frequencies, both coupled and uncoupled, were used in the analysis. These mode shapes, for two frequency ratios, are given in table IV. The distributed mass, static-unbalance, and moment-of-inertia properties needed in the calculation are given in table III. The oscillatory aerodynamic forces used in this analysis were obtained from piston theory (ref. 3) which has been presented for use at very high Mach numbers and low reduced frequencies. This aerodynamic theory permits the inclusion of nonlinear effects of airfoil shape and thickness in the flutter analysis. For some cases, the measured value of structural damping in each mode was included in the calculations.

RESULTS AND DISCUSSION

Experimental Results

The test-program results are shown chronologically in table V. This table shows the model frequencies and the test-section conditions either at flutter or at the maximum dynamic pressure if no flutter was obtained. For most of the tests when flutter was obtained, the test-section conditions are listed for both starting and stopping flutter. The stiffness-altitude parameter $\frac{b_r \omega_\theta}{a} \sqrt{\mu}$ is also given at flutter or at the maximum dynamic pressure.

As mentioned previously, it was found on some tests that the dynamic pressure at the end of flutter was as much as 50 percent less than the dynamic pressure at the start of flutter. This is shown in figure 6 where dynamic pressure at both the beginning and the end of flutter is plotted against Mach number for plan-form 2 with a frequency ratio of 1.02. When testing in the second mode of tunnel operation ($2.2 \lesssim M \lesssim 2.87$) which has a higher level of turbulence, flutter was found to begin much closer to the dynamic pressure where the flutter stopped than when testing at lower Mach numbers. This indicated the possibility that introducing some artificial turbulence into the airstream might produce results that are more consistent. Consequently, on all tests after test 20, turbulence was induced in the airstream by bleeding in air upstream of the test section.

With the flow upset in this manner, flutter could be started at much lower dynamic pressures than previously. This may have been due to nonlinearities in the system such as free play, nonlinear springs, nonlinear damping due to bearing supports (sometimes known as stiction), and so forth. However, experience with bearing supports has shown that their damping characteristics very often are highly nonlinear, and this factor probably accounts for the dependence of the system on turbulence level to initiate flutter.

Correlation was good for the end of flutter on tests both with and without turbulent flow at the same Mach number (for example, tests 18 and 22 in table V). For this reason, and since it is desirable to be conservative in predicting flutter, the flutter boundary is interpreted as being the dynamic pressure at which flutter stops.

Plan-form 1.- Only one flutter point was found with plan-form 1. This one point (test 7) was at a Mach number of 2.21 and occurred at the extreme upper limit of dynamic pressure available. The model stiffness gave an uncoupled-frequency ratio of 1.12, the frequency ratio nearest 1 which was tried on this configuration. When a heavy leading edge was added, increasing the model weight by 20 percent and changing the frequency ratio to 1.16 eliminated the flutter point as shown by test 51 in table V.

Plan-form 2.- As shown in figure 7, flutter was obtained on plan-form 2 between Mach numbers of 1.49 to 2.80. For a ratio of uncoupled bending frequency to uncoupled pitching frequency of 1.02, flutter points were determined over this entire Mach number range and an indication of constant dynamic-pressure flutter was found at the higher Mach numbers. At frequency ratios of 0.91 and 1.41, flutter was found only over part of the Mach number range; and at a frequency ratio of 0.82 (see table V) no flutter was found within the operating limits of the tunnel. The trend of the flutter boundary with Mach number is different for the various frequency ratios, and the dynamic pressure at flutter is much lower when the frequency ratio is near 1.

A mass balance of about 7 percent of the basic-control weight was distributed over the outboard 48 percent span of the leading edge of the model. This distribution changed the uncoupled-frequency ratio from 1.02 to 0.95. The test results are shown in figure 7 and indicate that dynamic pressure at flutter is at least doubled by adding the balance weight. The flutter boundary is similar to the boundary for the unbalanced model with a frequency ratio of 0.91. Thus, the improvement in flutter characteristics with mass balance can be attributed to the frequency-ratio change as well as to the center-of-gravity shift. A similarly balanced model with a frequency ratio of 0.89 would not flutter at the maximum dynamic pressure available.

The variation of the ratio of flutter frequency to uncoupled pitching frequency with Mach number is shown in figure 8 for the various mass and frequency-ratio combinations on plan-form 2. In general, the flutter frequency falls between the uncoupled frequencies. An indication of the makeup of the flutter mode was obtained from high-speed motion pictures. The flutter mode for frequency ratios of 1.02 and 1.41 consisted of bending coupled with pitch. For a frequency ratio of 0.91, as well as for the mass-balanced case with a frequency ratio of 0.95, the flutter mode was predominately bending.

Plan-form 3.- Only a limited number of tests were conducted on plan-form 3, but the few data points obtained are shown in figure 9. Two flutter points were found at an uncoupled-frequency ratio of 1.00 on plan-form 3. A very mild flutter, predominately elevator rotation, occurred at the top dynamic pressure available at a Mach number of 2.80. A very violent flutter was found at a Mach number of 2.21. A violent-flutter point was also found when the frequency ratio was 0.88 at a Mach number of 1.61. No flutter points at much higher dynamic pressures were found at Mach numbers of 1.61 and 2.21 for an uncoupled-frequency ratio of 1.16. This would indicate that keeping the bending frequency above the pitching frequency would be beneficial in this range of frequency ratios. Divergence was too rapid on the violent-flutter cases for motion pictures to be taken to determine the flutter modes.

Calculations

The results of flutter calculations on plan-form 2 at a frequency ratio of 1.02 are shown in figures 10 and 11. These calculations, which were made by use of piston theory with the effect of thickness included, used both coupled and uncoupled measured modes with both zero damping and measured damping in each mode. The flutter frequency calculated by use of all four procedures was within 5 percent of the experimental value, as shown in figure 10 where the ratio of calculated flutter frequency to experimental flutter frequency is plotted against Mach number. The ratio of calculated flutter velocity to experimental flutter velocity plotted against Mach number, shown in figure 11, varied considerably with the calculation procedure. Coupled modes used with zero structural damping gave the best results - within 3 percent of experiment. The other methods gave results which were off by as much as 45 percent. The addition of damping increased the calculated flutter velocity by a large amount.

It should be noted that the center of gravity for this plan form is very near the axis of rotation. The uncoupled-mode analysis is probably more sensitive to errors in this distance; thus, the coupled-mode analysis is the preferred method.

The coupled-mode, zero-structural-damping calculation for plan-form 2 at a frequency ratio of 1.02 is repeated in figure 12 as the stiffness-altitude parameter plotted against Mach number and is compared with experimental data points. Also shown in the figure are the results of a similar calculation on plan-form 2 at a frequency ratio of 1.41. The calculations at a frequency ratio of 1.41 do not show the same good agreement with experiment as those at a frequency ratio of 1.02.

These calculations have been made by using piston theory. The effects of airfoil shape and thickness have been included in the calculations presented. The calculations were also made for zero thickness, and very little effect was found for the frequency ratios near 1. The thickness trends with frequency ratio were the same as those pointed out in reference 4.

SUMMARY OF RESULTS

From a supersonic flutter investigation of three low-aspect-ratio control surfaces, the following results were obtained:

1. The single flutter point found on plan-form 1 was eliminated by adding a distributed mass balance along the leading edge of the control. This mass balance increased the basic-control weight by 20 percent.
2. Plan-form 2 fluttered at lower dynamic pressures when the ratio of uncoupled bending frequency to uncoupled pitching frequency was near 1. The flutter dynamic pressure was at least doubled for all Mach numbers when the frequency ratio was changed from 1.02 to 0.82, 0.91, or 1.41. The flutter boundaries for three frequency ratios all showed different trends with Mach number.
3. A mass balance of 7 percent of the elevator weight, distributed over the outboard 48 percent span of the leading edge, at least doubled the dynamic pressure at flutter on one stiffness configuration for plan-form 2. This improvement in flutter characteristics may be due to the change in frequency ratio as well as to the shift of the center of gravity.
4. Plan-form 3 exhibited violent, destructive flutter. The largest flutter margins on this plan form were obtained when the uncoupled bending frequency was above the uncoupled pitching frequency.
5. Calculations using piston theory gave good agreement with experiment on plan-form 2 with a frequency ratio of 1.02 when either uncoupled

modes with structural damping or coupled modes without damping were used. Calculated results at a frequency ratio of 1.41 deviated considerably from experiment.

Langley Aeronautical Laboratory,
National Advisory Committee for Aeronautics,
Langley Field, Va., February 10, 1958.

REFERENCES

1. Boswinkle, Robert W., Jr., and Morgan, Homer G.: Flutter Experiments With Various Control Configurations. NACA RM L57D23c, 1957.
2. Scanlan, Robert H., and Rosenbaum, Robert: Introduction to the Study of Aircraft Vibration and Flutter. The MacMillan Co., 1951.
3. Ashley, Holt, and Zartarian, Garabed: Piston Theory - A New Aerodynamic Tool for the Aeroelastician. Jour. Aero. Sci., vol. 23, no. 12, Dec. 1956, pp. 1109-1118.
4. Runyan, Harry L., and Morgan, Homer G.: Flutter at Very High Speeds. NACA RM L57D16a, 1957.

TABLE I

GEOMETRIC CHARACTERISTICS OF MODELS

Plan form	Total area, sq ft	Ratio of fixed-surface area to movable-surface area	Mean aerodynamic chord, ft	Panel aspect ratio	Hinge line, fraction of mean aerodynamic chord	Thickness, fraction of chord
1	3.10	0	2.16	1.06	0.38	0.05
2	2.88	0	1.63	1.62	.45	.06 to .035
3	3.28	.25	2.04	1.00	.42	.03

TABLE II

MODEL MASS DATA^a

Plan form	Model	Mass-balance configuration	Total weight, lb	Balance weight, lb	Boom weight, lb	Center of gravity		Pitch inertia about hinge line, lb-ft ²	Flapping inertia about center of gravity, lb-ft ²	Product of inertia about center of gravity, lb-ft ²
						Distance from root, ft	Distance rearward of hinge line, ft			
1	a	None	5.78			0.45	0.088	1.54	1.08	0.456
	b	Boom-mounted balance weight	6.85	0.88	0.21	.54	.044	2.13	1.43	.021
	c	Heavy leading edge	7.03			.51	.042	2.31	1.60	.133
2	a	None	7.40			.56	.009	1.15	2.66	
	b	None	7.32			.57	.002	1.09	2.72	
	c	Heavy leading edge	7.91	.50		.63	.016	1.21	3.32	
	d	Heavy leading edge	7.75	.54		.64	.023	1.16	3.32	
3	a	None	6.63			.59	.158	2.08	2.38	.905
	b	None	6.67			.62	.157	2.02	1.52	.908

^aThe weights do not include the torsion spring or any portion of the spindle outside the surface. The product of inertia is calculated. All other data are measured.

TABLE III

COMPUTED DISTRIBUTED MASS, STATIC UNBALANCE, AND MOMENT
OF INERTIA OF PLAN-FORM 2 WITHOUT MASS BALANCE

Span interval, fraction of span	m, slugs/ft	S_{θ} , $\frac{\text{slug-ft}}{\text{ft}}$	I_{θ} , $\frac{\text{slug-ft}^2}{\text{ft}}$
0 to 0.055	0.4262	0.00854	0.0615
.055 to .167	.3096	.00618	.0442
.167 to .278	.0732	.00097	.0117
.278 to .389	.1138	.00151	.0182
.389 to .500	.0867	.00188	.0142
.500 to .611	.0399	.00096	.00654
.611 to .722	.0613	.00158	.00976
.722 to .833	.0455	.00175	.00675
.833 to .944	.0294	.00129	.00468
.944 to 1.0	.0135	.00069	.00226

TABLE IV
 MEASURED MODE SHAPES FOR PLAN-FORM 2
 WITHOUT MASS BALANCE

(a) Uncoupled modes

η , fraction of span	$\omega_h/\omega_\theta = 1.02$		$\omega_h/\omega_\theta = 1.41$	
	$F_h, f_h = 70$ cps	$F_\theta, f_\theta = 68.5$ cps	$F_h, f_h = 72$ cps	$F_\theta, f_\theta = 51$ cps
0	0.088	1.000	0.072	1.000
.2	.149	1.041	.137	1.005
.4	.268	1.045	.264	.963
.6	.451	1.014	.454	.908
.8	.695	.891	.698	.841
1.0	1.000	.632	1.000	.771

(b) Coupled modes for $\omega_h/\omega_\theta = 1.02$

η , fraction of span	F_{h1}	$F_{\theta1}$	F_{h2}	$F_{\theta2}$
	$f_1 = 61$ cps		$f_2 = 72$ cps	
0	0.041	0.0712	0.015	-0.0599
.2	.117	.0748	.072	-.0643
.4	.213	.0743	.174	-.0652
.6	.379	.0706	.344	-.0601
.8	.628	.0653	.599	-.0450
1.0	1.000	.0590	1.000	-.0144

(c) Coupled modes for $\omega_h/\omega_\theta = 1.41$

η , fraction of span	F_{h1}	$F_{\theta1}$	F_{h2}	$F_{\theta2}$
	$f_1 = 45$ cps		$f_2 = 69$ cps	
0	0.186	0.435	0.045	-0.0050
.2	.473	.410	.143	-.0051
.4	.685	.392	.287	-.0057
.6	.834	.382	.467	-.0068
.8	.934	.378	.700	-.0086
1.0	1.000	.377	1.000	-.0113

TABLE V.- COMPILATION OF TEST RESULTS

Test	Plan form	Model	Pitching frequency, cps	$\frac{\omega_h}{\omega_\theta}$	M	q, lb/sq ft	V, fps	ρ , slugs/cu ft	μ	$\frac{b_r \omega_\theta}{a} \sqrt{\mu}$	$\frac{\omega_r}{\omega_\theta}$	Remarks
1 2 3 4 5	1	b b b a a	51.1 51.1 51.1 60.5 60.5	1.30 1.30 1.30 1.52 1.52	1.61 2.21 2.80 1.60 2.20	2,038.7 2,281.8 1,424.0 2,097.2 2,570.6	1,591 1,914 2,122 1,579 1,989	.001611 .001246 .000632 .001682 .001300	24.1 31.1 61.4 19.4 25.1	1.72 2.24 3.59 1.84 2.28		No flutter
6 7 8 9 10	1	a	88.4 88.4 88.4 51.0 51.0	1.12 1.12 1.12 1.76 1.76	1.60 2.21 2.80 2.21 1.60	2,089.9 2,620.0 1,451.9 2,586.4 2,075.4	1,579 1,907 2,119 1,906 1,579	.001682 .001441 .000647 .001424 .001664	19.5 22.7 50.6 23.0 19.6	1.72 3.31 5.65 1.93 1.56	1.23	No flutter Flutter at maximum tunnel conditions No flutter No flutter No flutter
11(a) 11(b) 14(a) 14(b) 15(a) 15(b)	2	a	68.5	1.02	1.59 1.59 1.75 1.68 2.80 2.80	368.7 303.0 866.3 402.7 781.0 770.5	1,571 1,571 1,671 1,629 2,119 2,119	.000299 .000245 .000620 .000304 .000348 .000343	254.6 205.9 182.1	5.65 5.19 6.26	1.00 1.03 1.00	Flutter begins Flutter stops Flutter begins Flutter stops Flutter begins Flutter stops
16 17(a) 17(b) 18(a) 18(b)	2	a	91.8 68.5 68.5 68.5 68.5	0.82 1.02 1.02 1.02 1.02	1.60 1.49 1.49 1.60 1.60	2,115.4 475.2 311.8 816.0 371.6	1,579 1,498 1,498 1,582 1,584	.001696 .000423 .000278 .000652 .000296	36.8 225.0 — 211.1	2.89 5.22 5.15	1.01 1.03	No flutter Flutter begins Flutter stops Flutter begins Flutter stops
19(a) 19(b) 20(a) 20(b) 21(a) 21(b)	2	a	68.5	1.02	1.91 1.90 2.00 1.99 2.21 2.21	1,114.2 488.3 1,258.4 506.8 687.2 608.4	1,769 1,764 1,817 1,814 1,926 1,913	.000718 .000314 .000763 .000308 .000371 .000332	199.2 203.0 188.0	5.34 5.48 5.55	1.03 1.03 1.00	Flutter begins Flutter stops Flutter begins Flutter stops Flutter begins Flutter stops
22(a) 22(b) 23(a) 23(b) 24(a) 24(b)	2	a	68.5 68.5 67.8 67.8 67.8 67.8	1.02	1.60 1.60 2.60 2.60 2.40 2.40	451.7 364.3 731.8 646.0 688.1 623.8	1,582 1,578 2,065 2,065 1,992 1,992	.000361 .000293 .000343 .000303 .000347 .000314	213.6 206.4 198.9	5.21 6.27 5.90	1.00 1.00 1.00	Flutter begins Flutter stops Flutter begins Flutter stops Flutter begins Flutter stops

TABLE V.- COMPILATION OF TEST RESULTS - Concluded

Test	Plan form	Model	Pitching frequency, cps	$\frac{\omega_h}{\omega_\theta}$	M	q, lb/sq ft	V, fps	ρ , slugs/cu ft	μ	$\frac{b_1^2 \omega_\theta}{a} \sqrt{\mu}$	$\frac{\omega_p}{\omega_\theta}$	Remarks				
25(a)	2	a	67.8	1.02	2.80	698.9	2,119	0.000311	215.9	6.74	1.00	Flutter begins Flutter stops No flutter No flutter				
25(b)			67.8	1.02	2.80	650.0	2,119	.000290								
26			91.8	.82	2.20	2,628.1	1,989	.001329					47.0	3.56		
27			50.7	1.41	1.61	2,063.1	1,586	.001641					38.1	1.63		
28(a)			50.9	1.41	2.21	1,588.1	1,904	.000876					75.9	2.63	1.33	Flutter begins Flutter stops
28(b)			50.9	1.41	2.21	1,492.4	1,904	.000823								
29	2	a	50.9	1.41	2.00	2,437.7	1,807	.001493	41.9	1.86	.75	No flutter No flutter No flutter No flutter Explosive flutter (lost model)				
30			50.9	1.41	2.80	1,457.2	2,119	.000649	96.3	3.38						
31			70.4	1.16	1.61	2,103.1	1,590	.001665	22.8	2.17						
32			70.4	1.16	2.21	2,638.6	1,912	.001444	26.3	2.66						
33			94.6	.88	1.61	1,020.7	1,590	.000808	67.1	5.04						
35	3	b	83.4	1.00	2.50	834.1	2,031	.000404	94.7	6.36	1.12	No flutter Mild flutter Explosive flutter (lost model)				
36		b	83.4	1.00	2.80	1,443.2	2,134	.000634	60.5	5.41						
37		b	83.4	1.00	2.21	1,661.7	1,918	.000903	42.4	3.99						
38	1	a	89.2	1.11	1.60	2,129.5	1,586	.001694	19.3	2.69	No flutter No flutter					
39		a	89.2	1.11	2.20	2,598.0	1,997	.001303	25.1	3.34						
40(a)	2	c	63.1	.95	1.61	872.2	1,591	.000689	107.9	3.39	.93	Flutter begins Flutter stops No flutter				
40(b)					1.61	785.0	1,591	.000620								
41					2.20	2,666.5	1,997	.001338					50.0	2.52		
42(a)					1.90	1,153.2	1,763	.000742					101.6	3.50	.94	Flutter begins Flutter stops No flutter (lost model when power failed)
42(b)					1.90	1,023.1	1,763	.000658								
43					2.10	2,614.4	1,883	.001475								
44	2	d	64.8	.89	2.87	884.8	2,138	.000387	168.9	5.77	.94	No flutter No flutter Flutter begins Flutter stops No flutter				
46		d	64.8	.89	1.60	1,726.6	1,591	.001365	47.9	2.31						
47(a)		b	76.5	.91	1.60	1,107.4	1,578	.000889	83.3	3.63						
47(b)		b	76.5	.91	1.60	925.2	1,578	.000743								
48		b	76.5	.91	1.90	2,412.1	1,757	.001563					39.6	2.67		
49(a)	2	b	76.5	.91	1.80	1,848.4	1,698	.001283	53.7	3.05	.96	Flutter begins Flutter stops No flutter No flutter No flutter No flutter				
49(b)		b	76.5	.91	1.80	1,654.1	1,693	.001154								
50		b	76.5	.91	2.20	2,690.7	1,989	.001361					45.5	2.92		
51		1	c	74.2	1.16	2.20	2,644.6	1,989					.001338	29.8	3.04	
52		1	c	74.2	1.16	1.61	1,940.6	1,584					.001546	25.7	2.60	

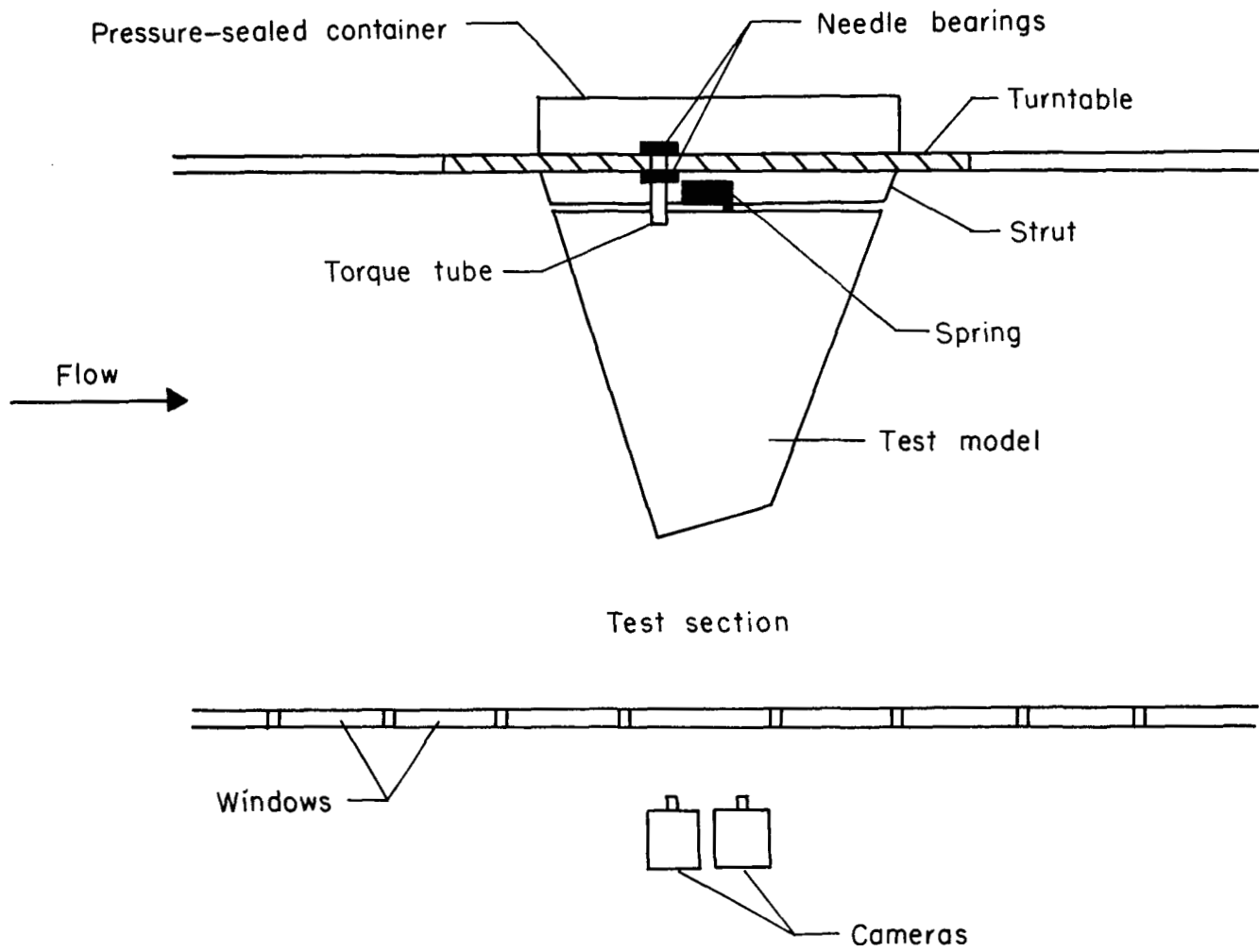
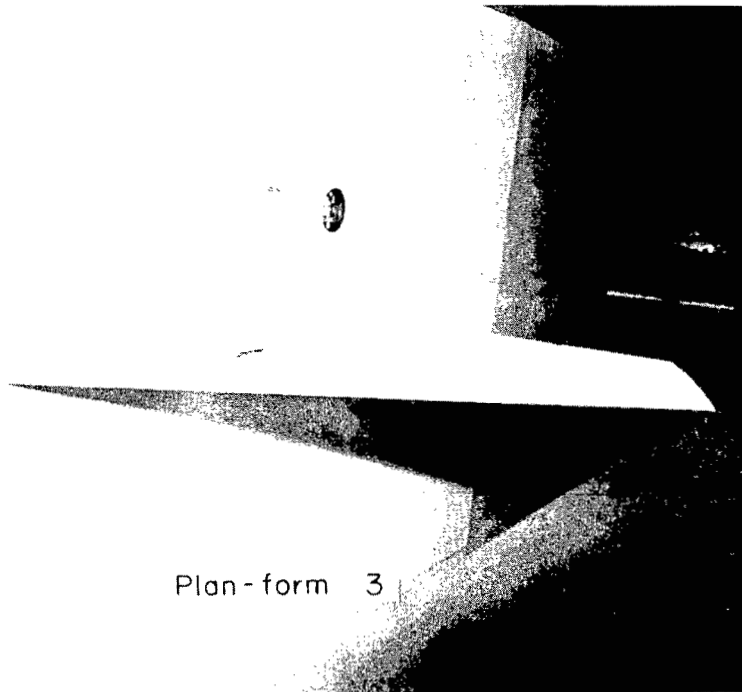
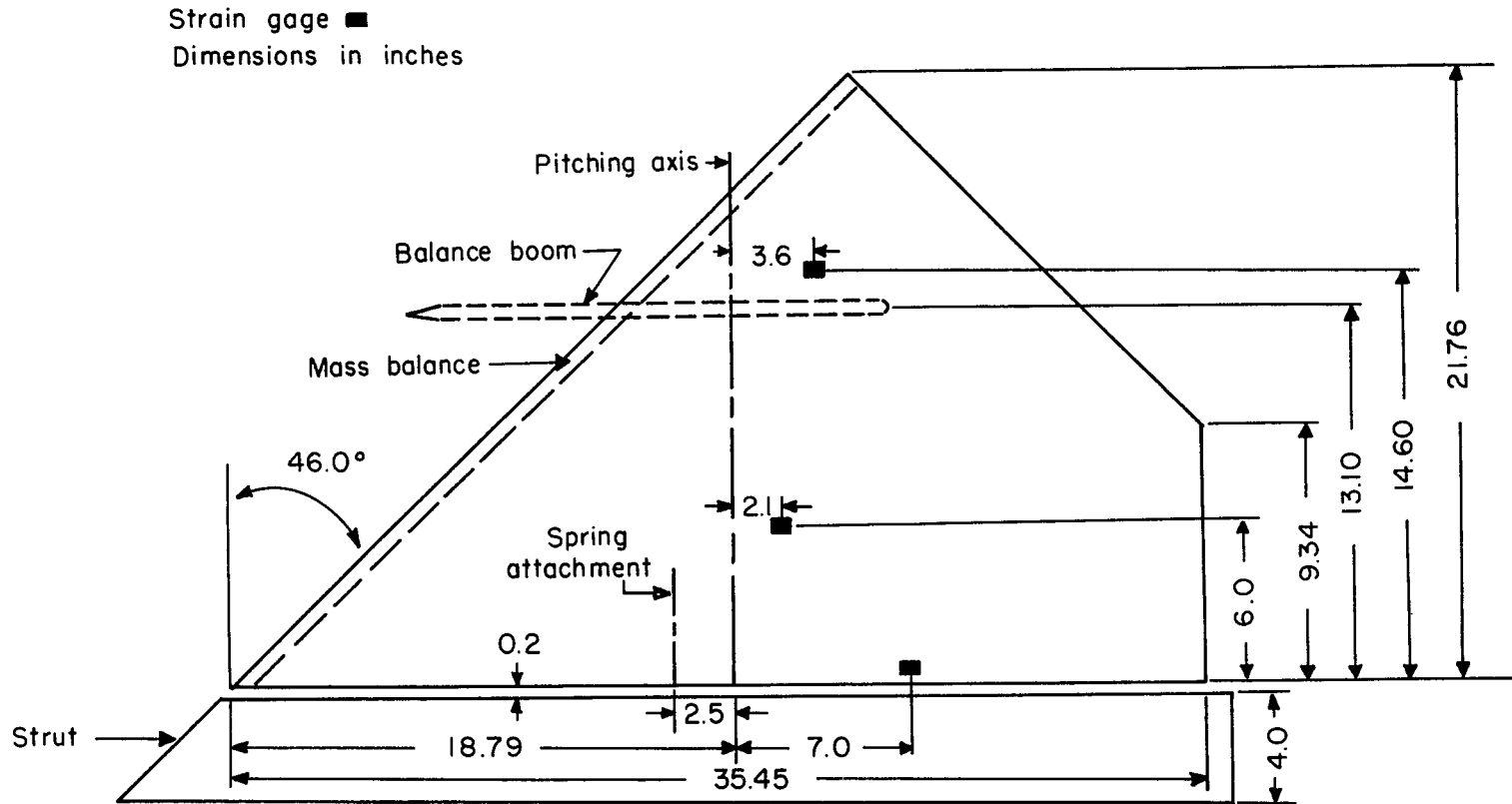


Figure 1.- Model and apparatus setup.



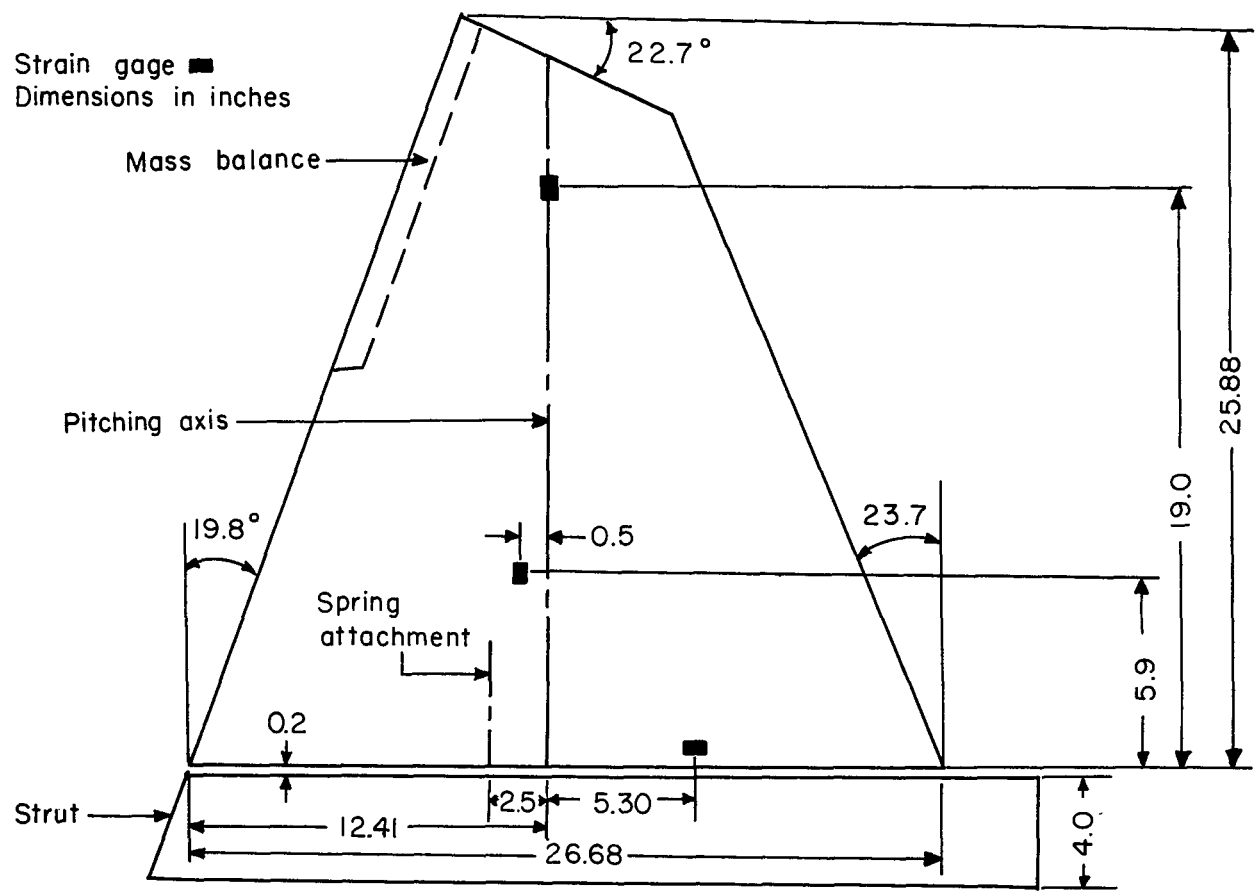
L-58-121

Figure 2.- Photograph of a model mounted in the test section of the Langley Unitary Plan wind tunnel.



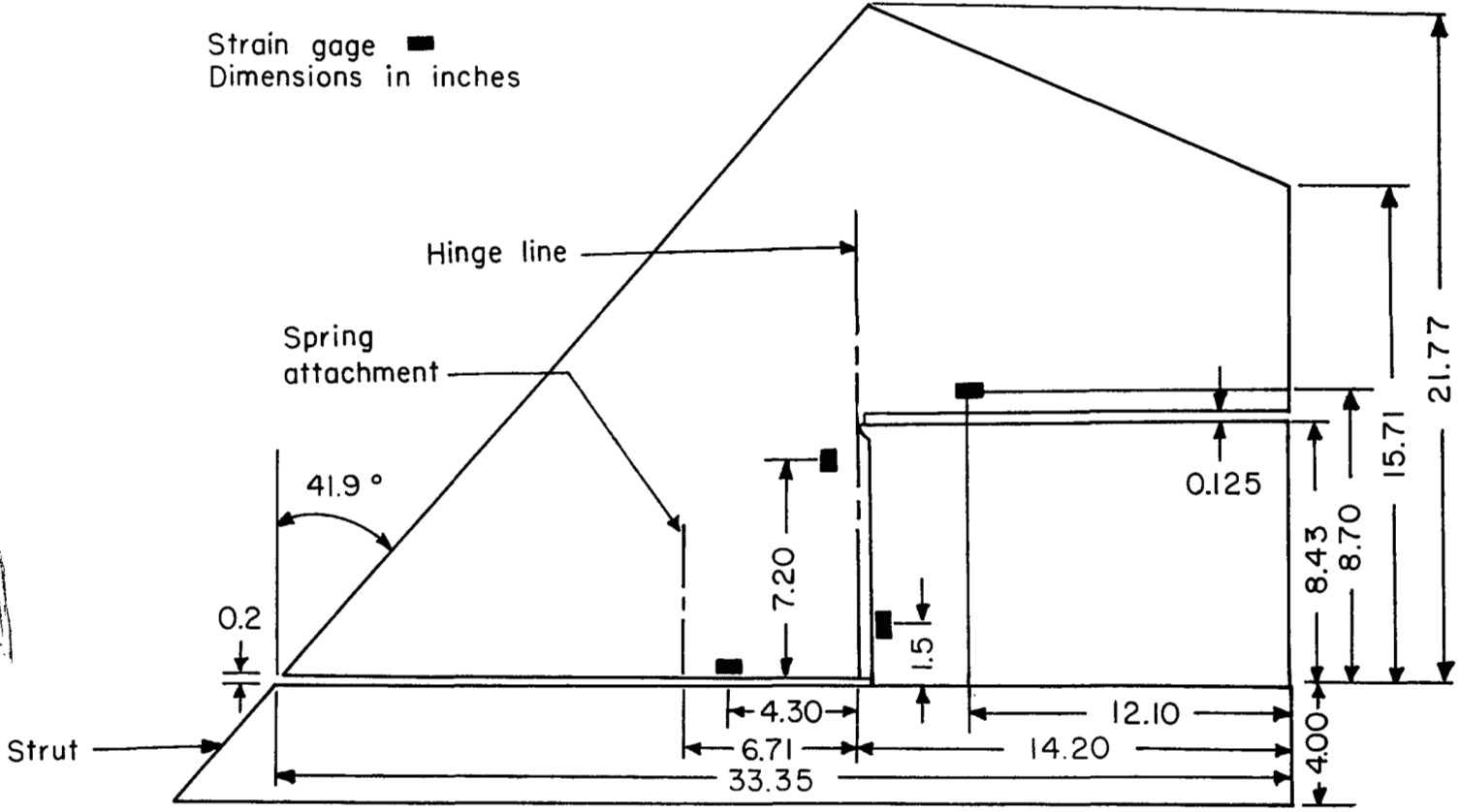
(a) Plan-form 1.

Figure 3.- Sketch of flutter models.



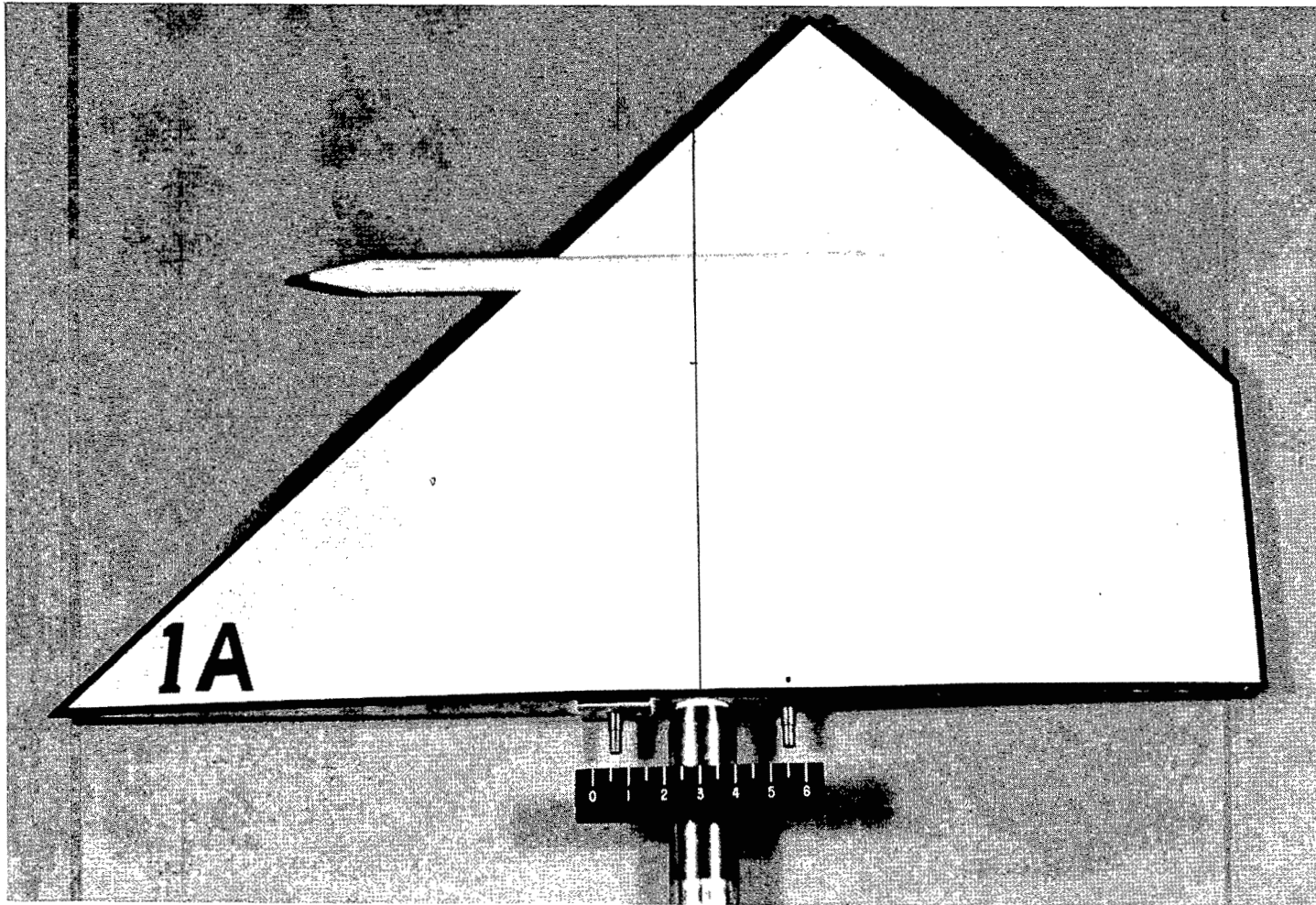
(b) Plan-form 2.

Figure 3.- Continued.



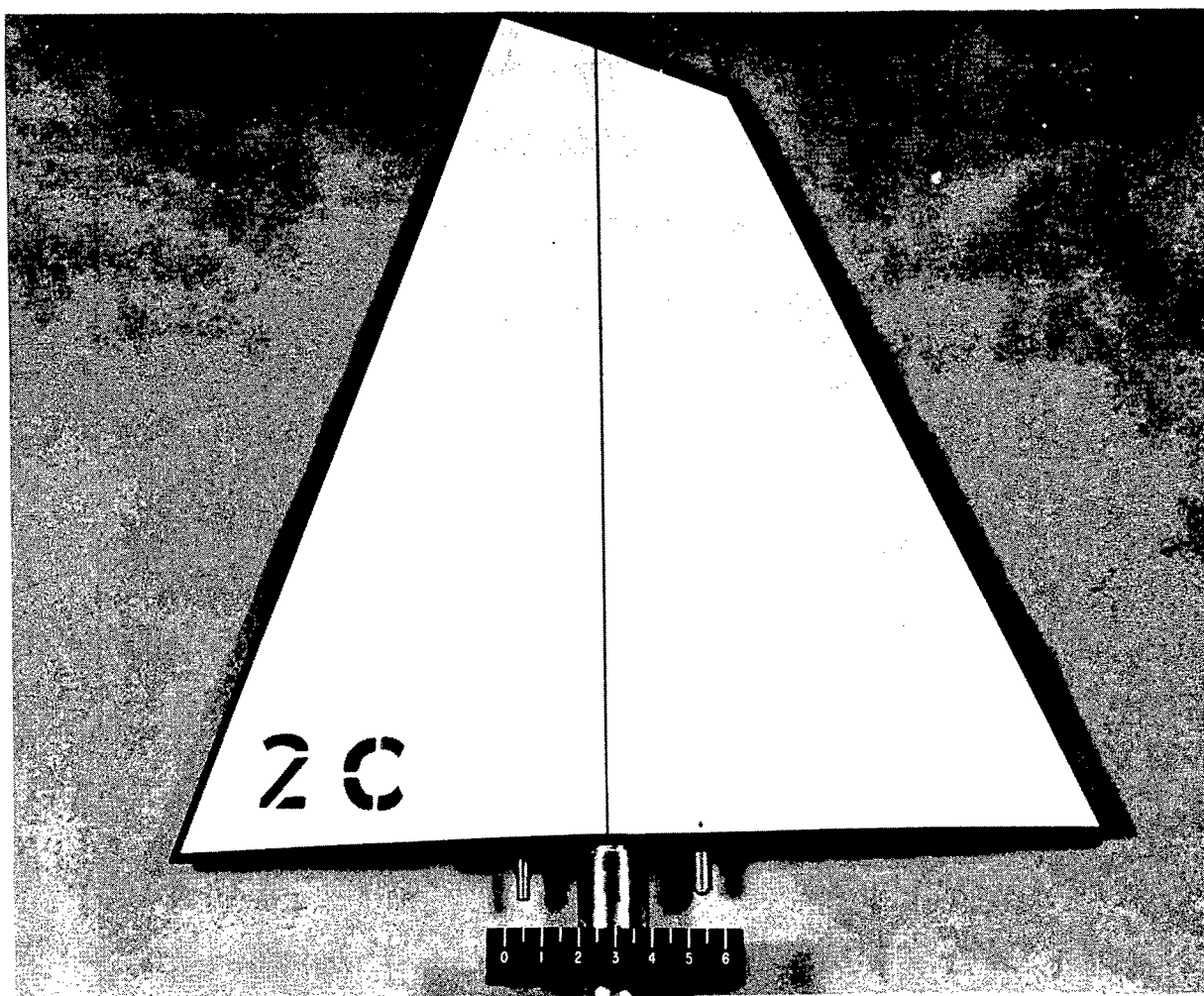
(c) Plan-form 3.

Figure 3.- Concluded.



(a) Plan-form 1 with a boom-mounted balance weight. L-97073

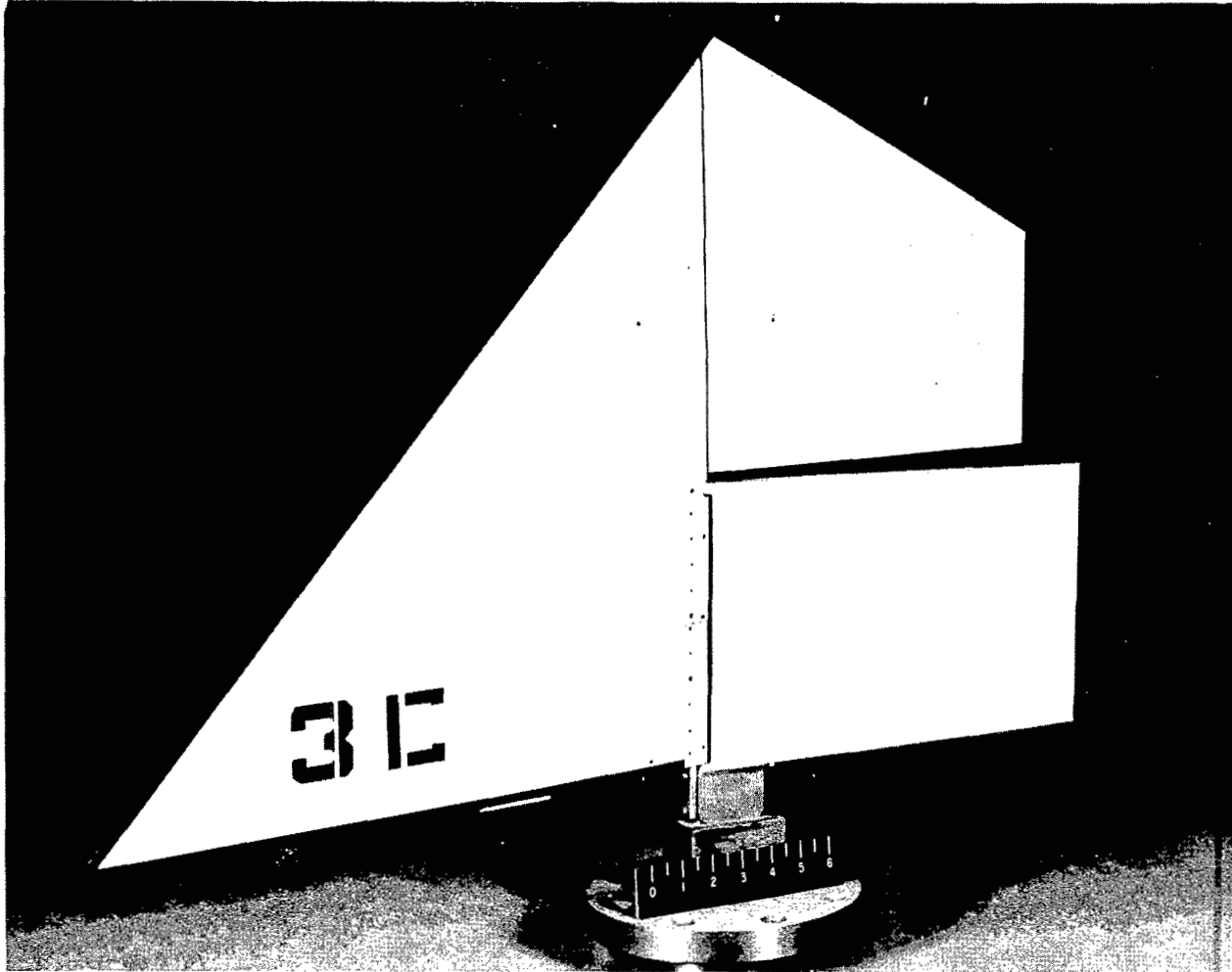
Figure 4.- Photographs of test models.



(b) Plan-form 2.

L-97074

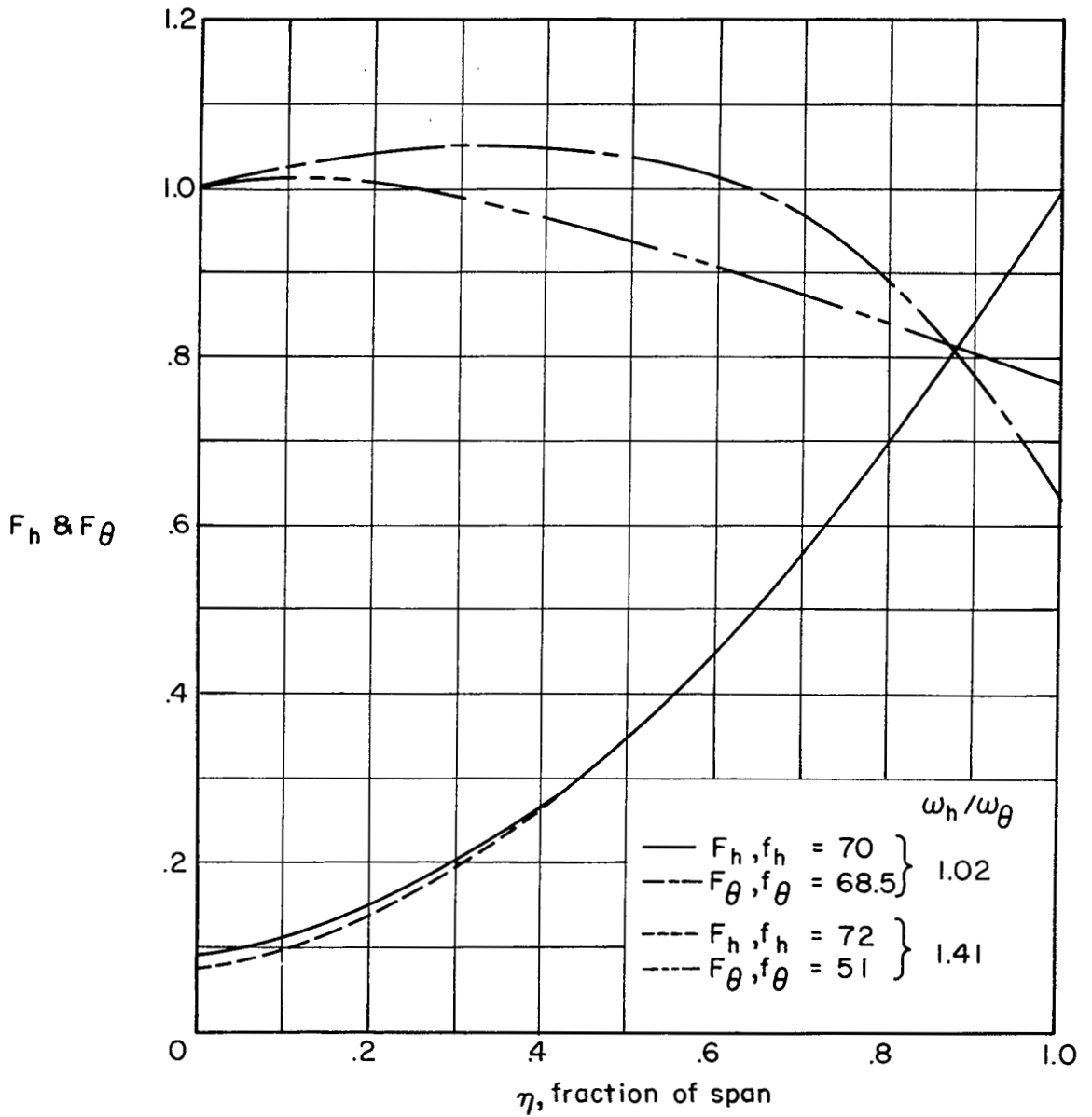
Figure 4.- Continued.



(c) Plan-form 3.

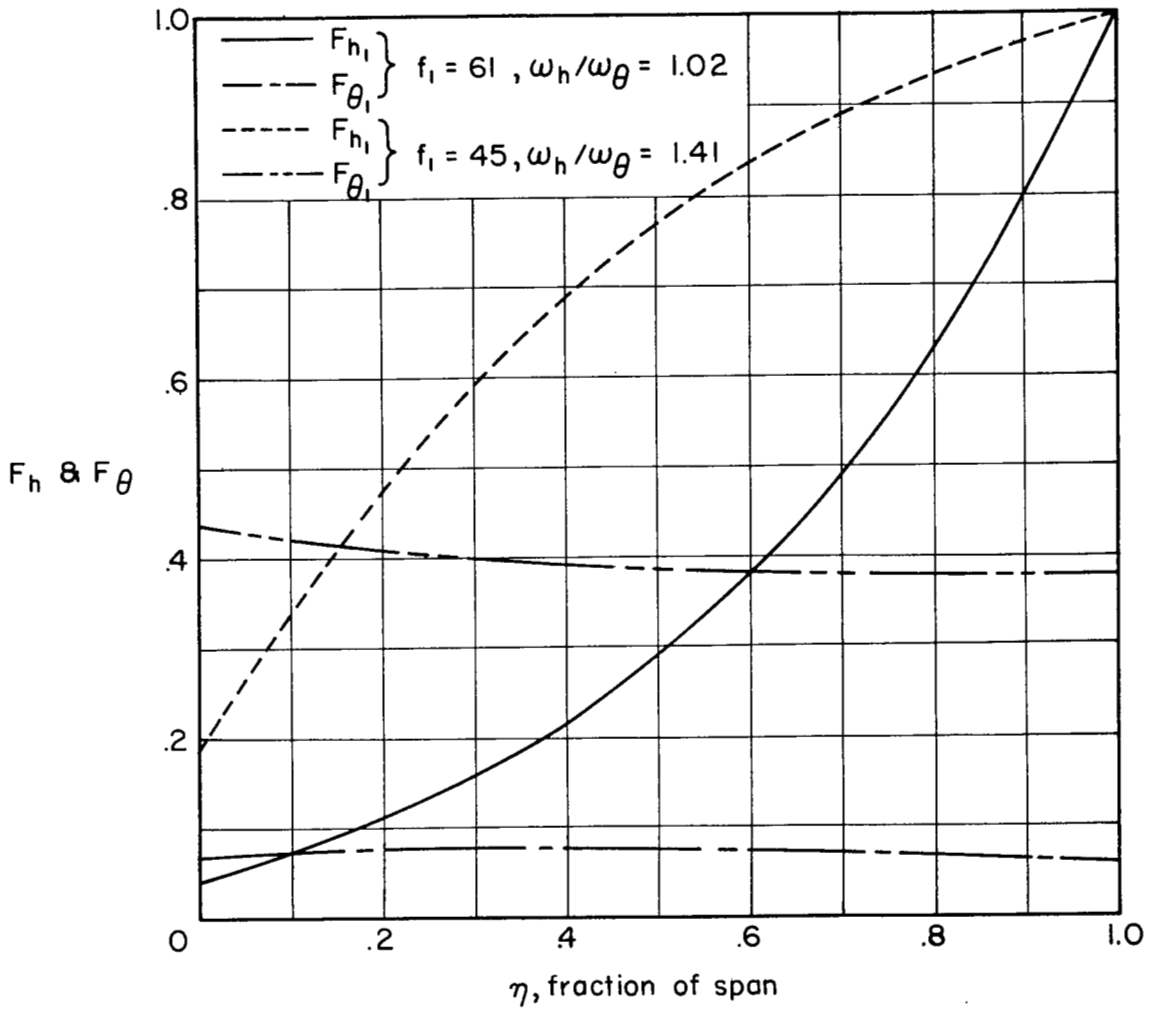
L-97076

Figure 4.- Concluded.



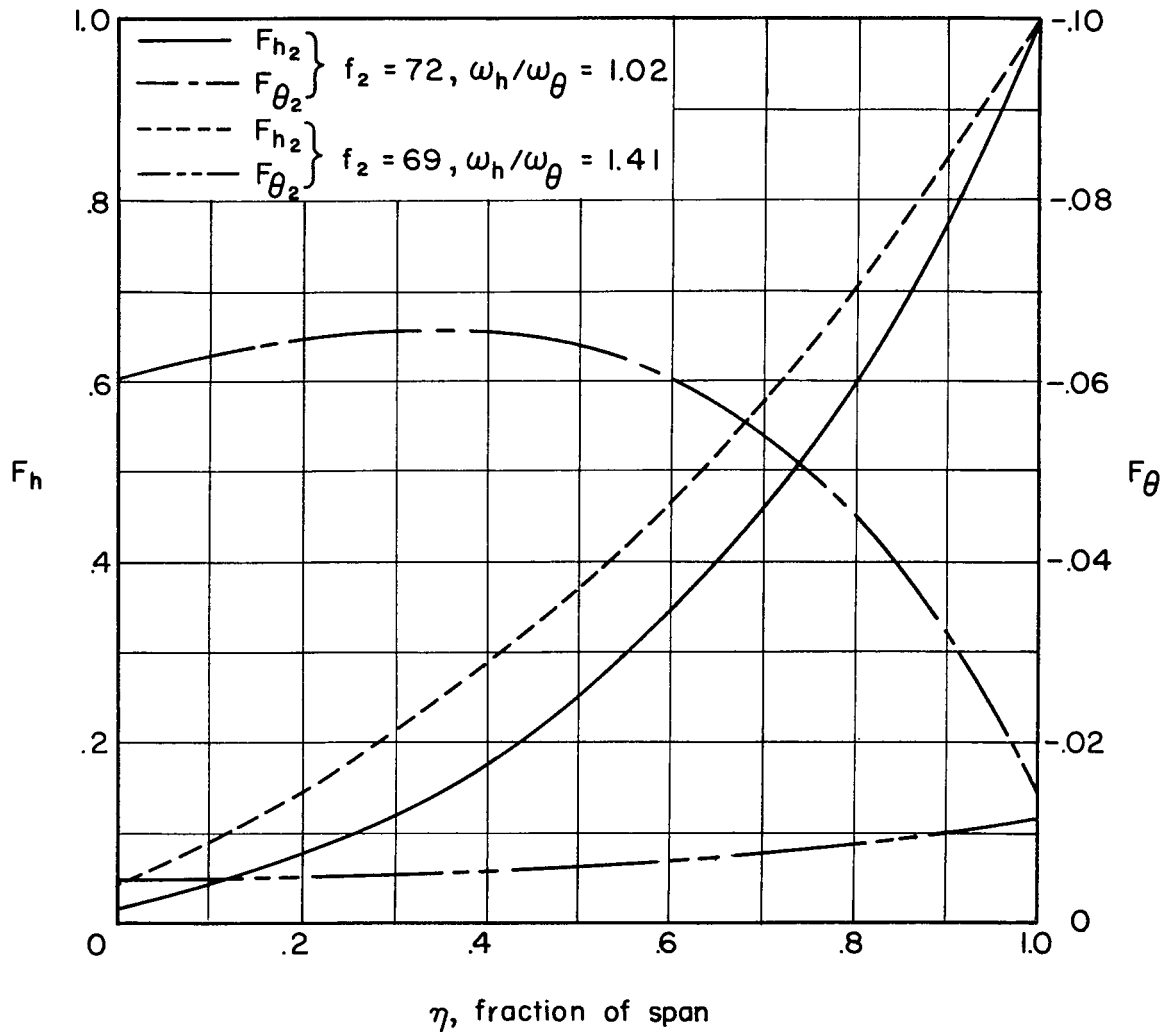
(a) Uncoupled bending- and pitching-mode shapes.

Figure 5.- Measured mode shapes for plan-form 2 at two frequency ratios.



(b) First coupled mode shapes at two frequency ratios.

Figure 5.- Continued.



(c) Second coupled mode shapes at two frequency ratios.

Figure 5.- Concluded.

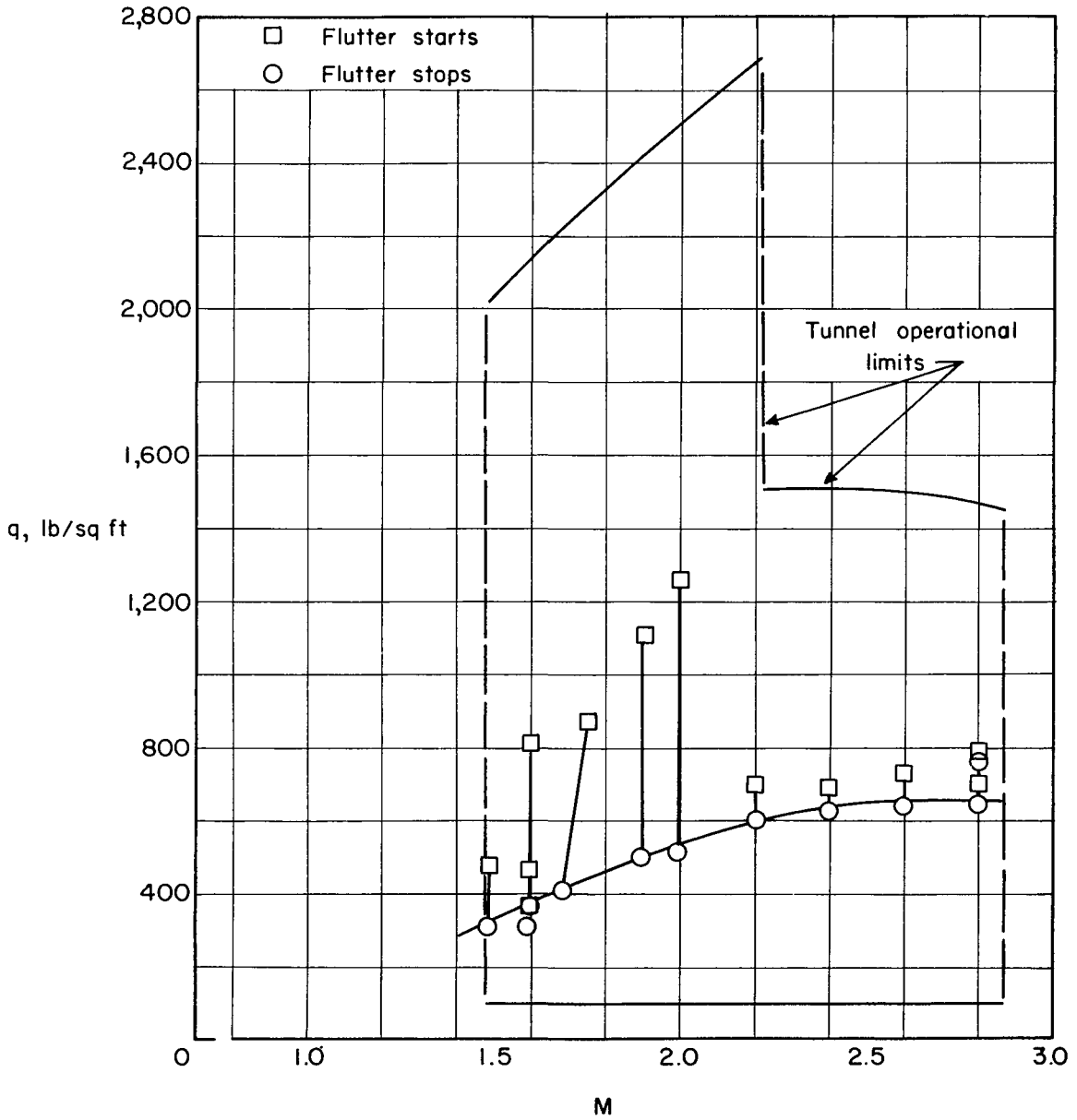


Figure 6.- Variation of dynamic pressure with Mach number for beginning and stopping of flutter for plan-form 2 with $\omega_h/\omega_\theta = 1.02$.

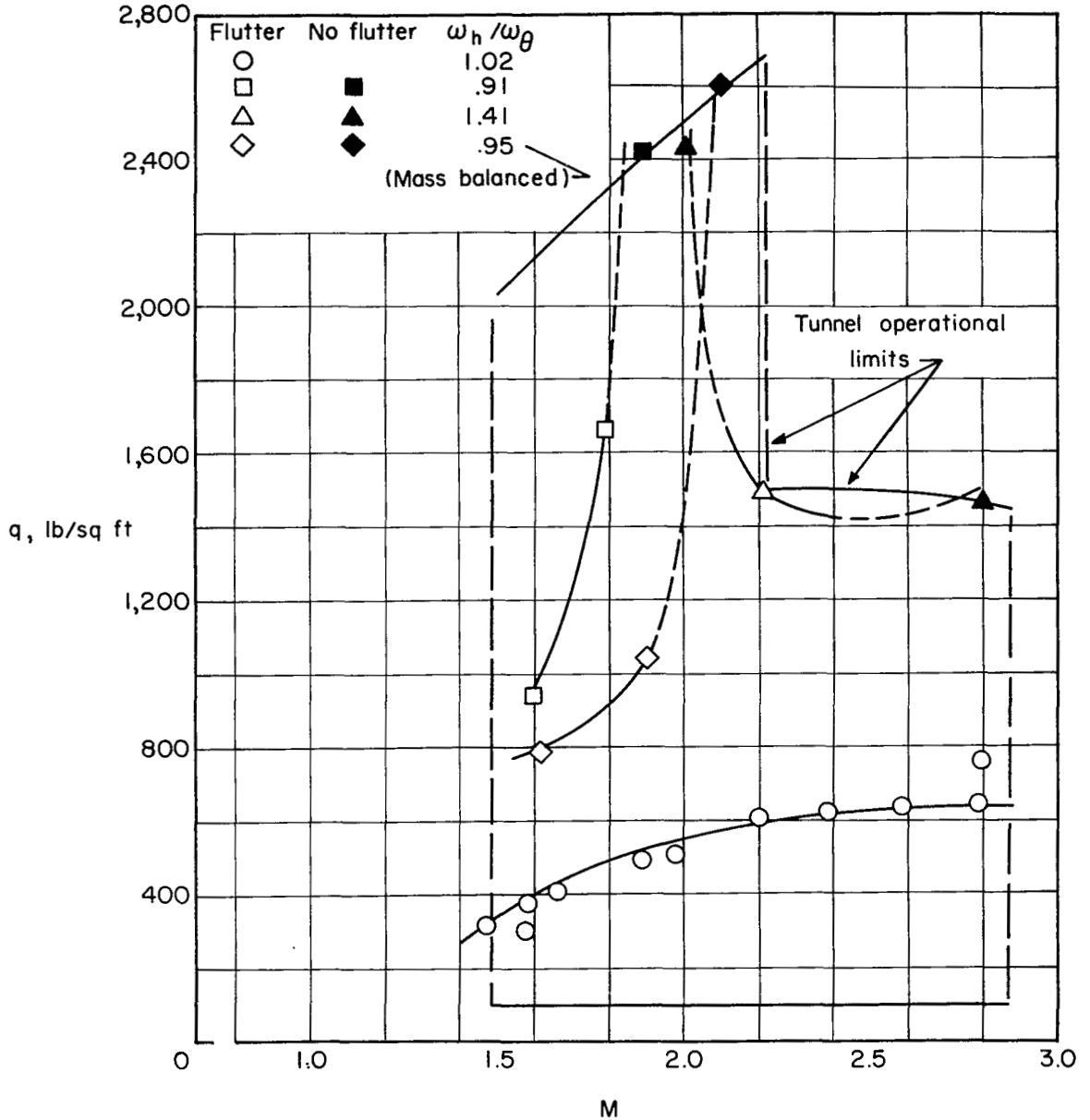


Figure 7.- Variation of dynamic pressure at flutter with Mach number for plan-form 2 at three frequency ratios and with mass balance added at one frequency ratio.

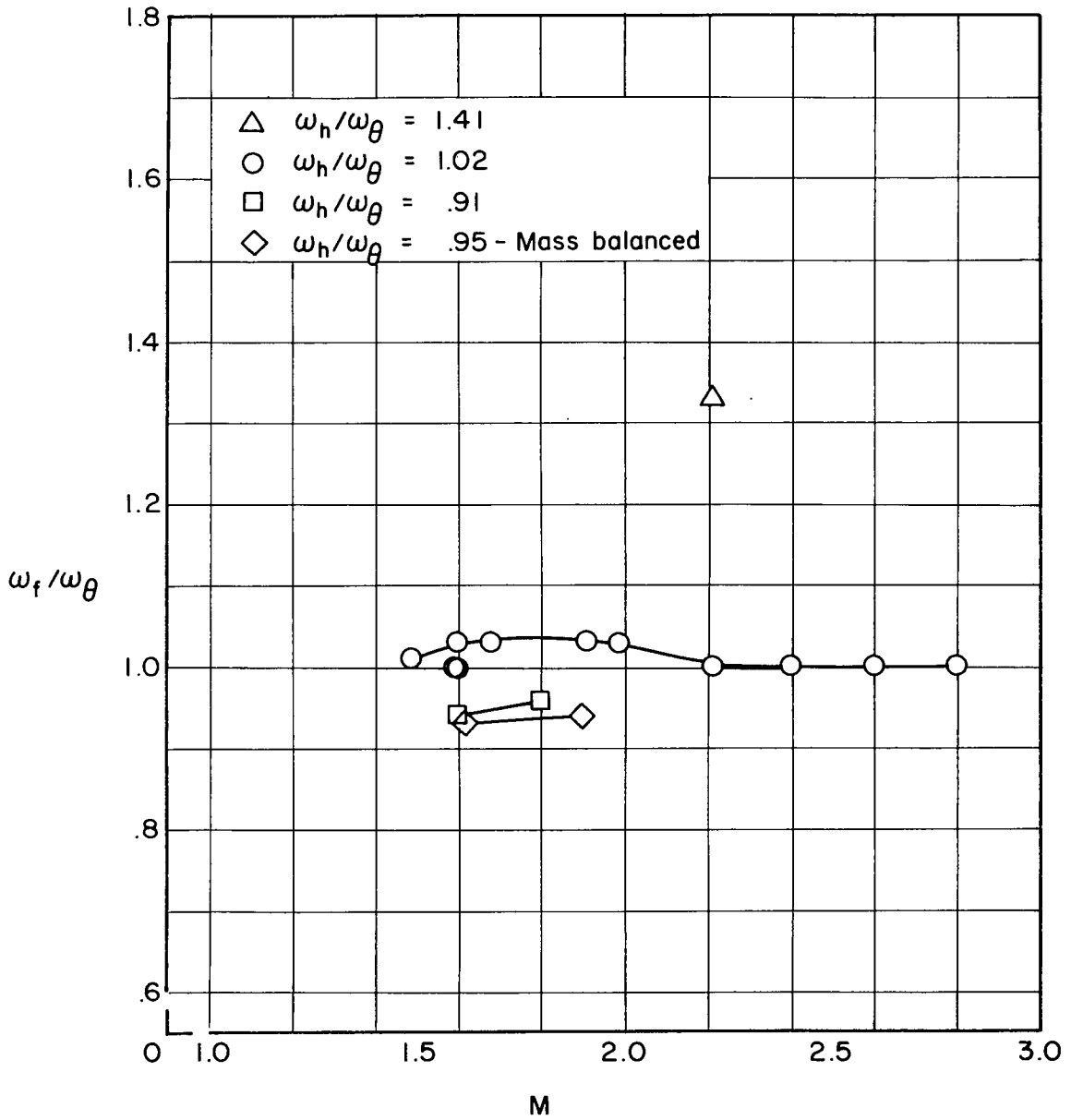


Figure 8.- Variation of ratio of flutter frequency to uncoupled pitching frequency with Mach number for plan-form 2.

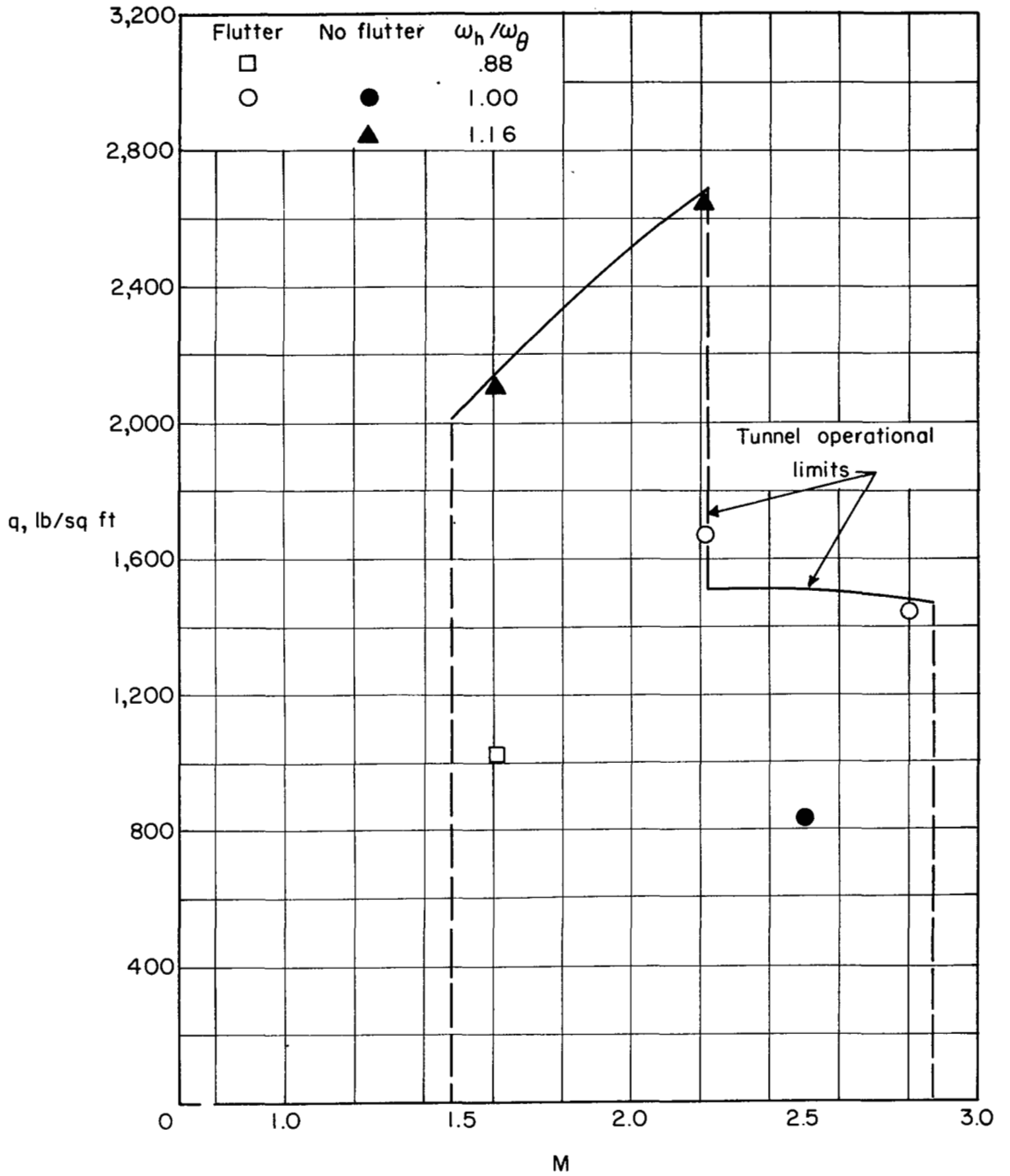


Figure 9.- Variation of dynamic pressure at flutter with Mach number for plan-form 3.

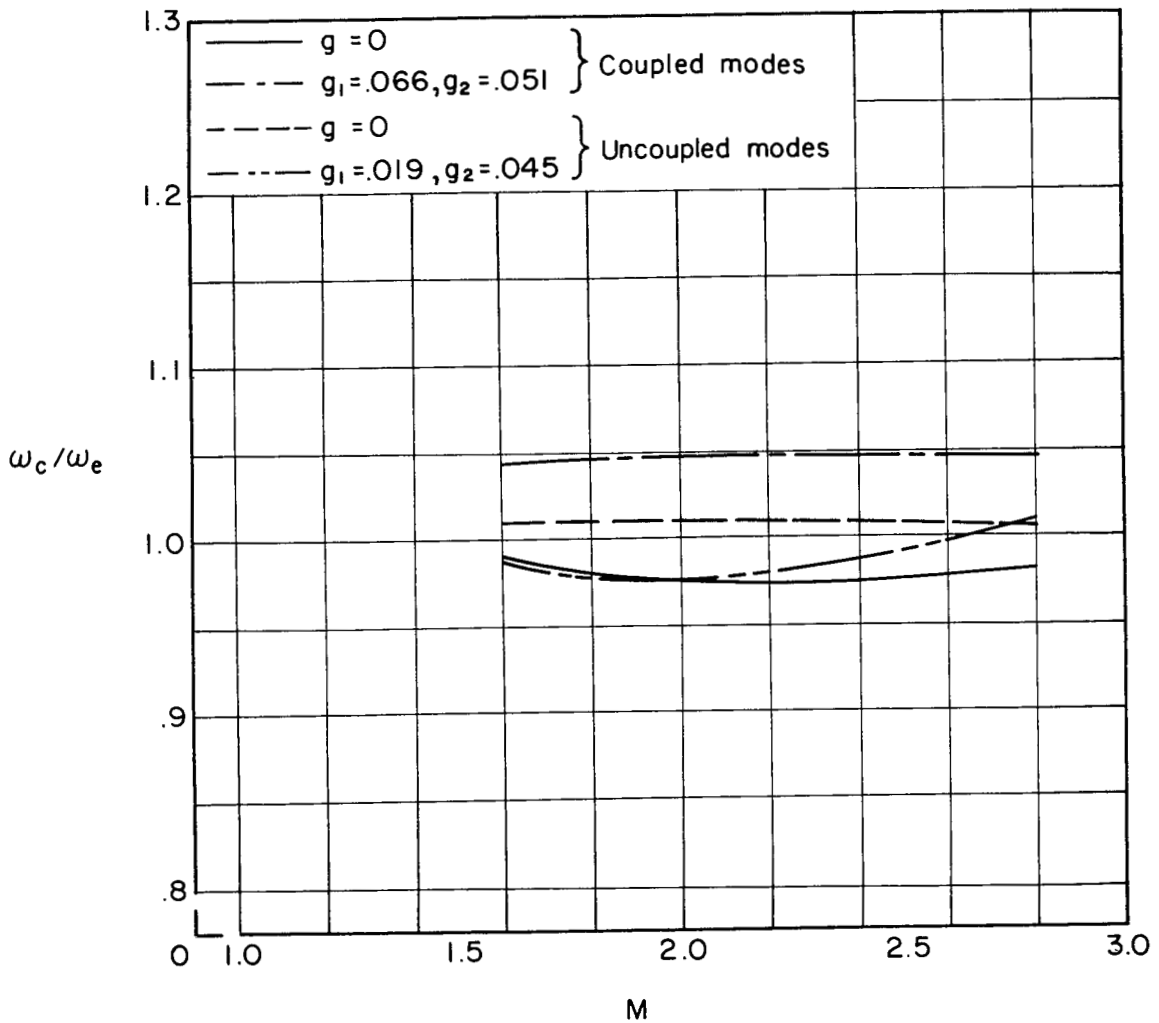


Figure 10.- Ratio of calculated flutter frequency to experimental flutter frequency plotted against Mach number for plan-form 2 with $\omega_h/\omega_\theta = 1.02$ by use of piston theory which includes thickness.

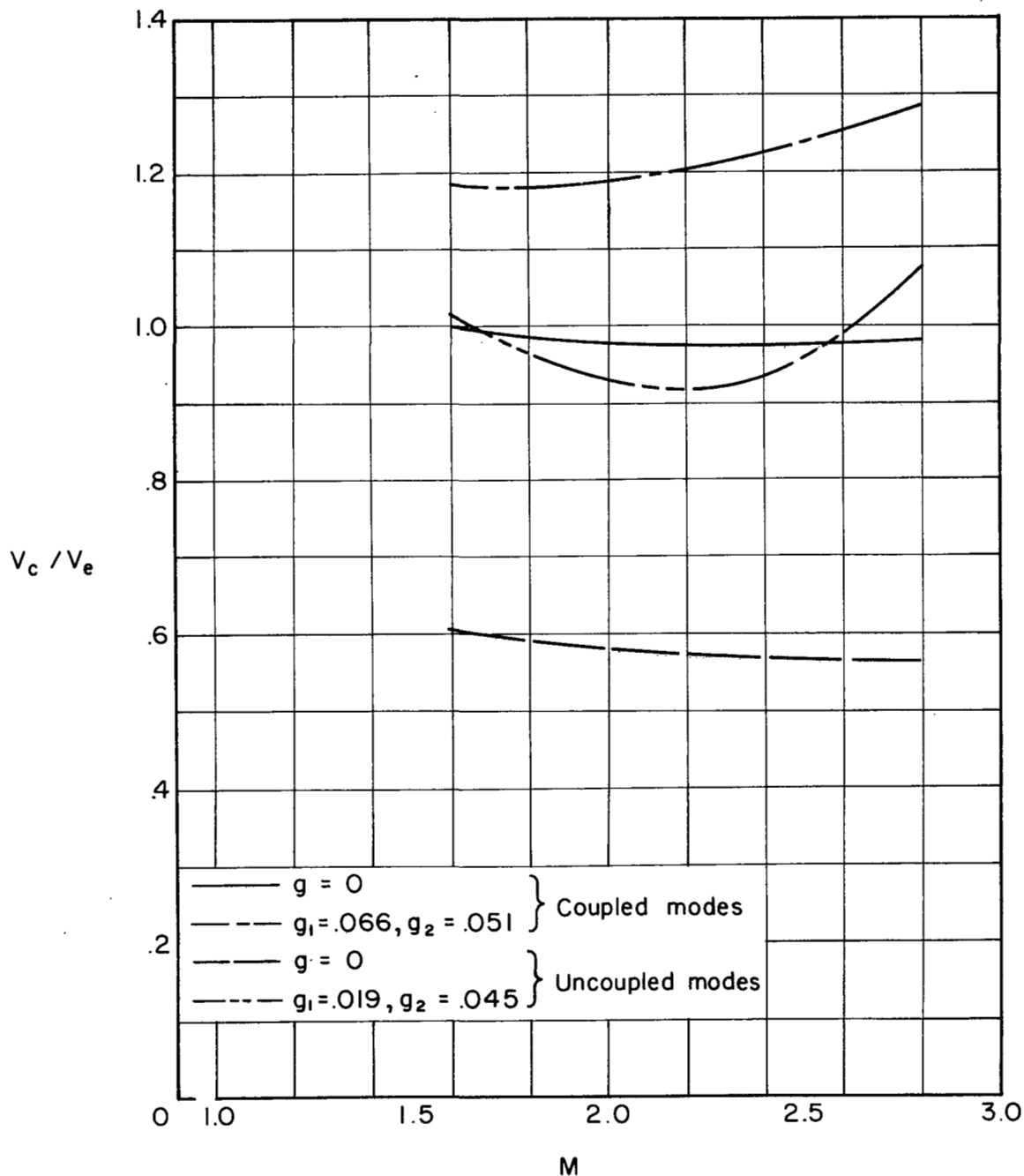


Figure 11.- Ratio of calculated flutter speed to experimental flutter speed plotted against Mach number for plan-form 2 with $\omega_h/\omega_\theta = 1.02$ by use of piston theory which includes thickness.

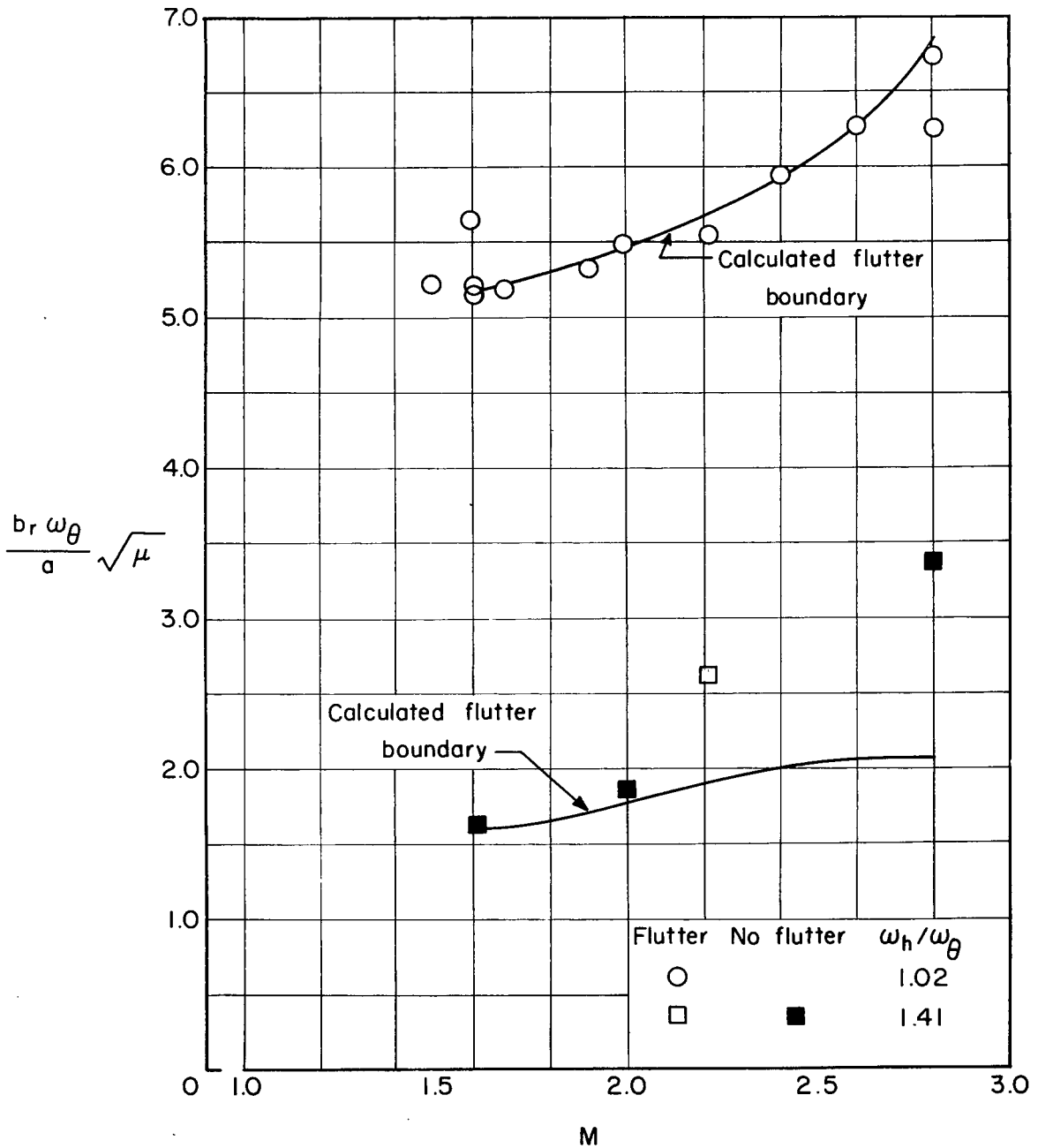


Figure 12.- Stiffness-altitude parameter plotted against Mach number for two frequency ratios on plan-form 2; comparison of experiment and coupled-mode calculations by use of zero structural damping and piston theory which includes thickness.

UNCLASSIFIED

~~CONFIDENTIAL~~

LANGLEY RESEARCH CENTER



3 1176 00511 2629

~~CONFIDENTIAL~~

UNCLASSIFIED